Joint Classified Bombs/Warheads & Ballistics Symposium
Monterey, California, August 4 – 7, 2014

WATER BARRIER PREDICTIONS FOR RIVERINE VESSEL DEFENSE (U)

William G. Szymczak(1), Raymond M. Gamache(2)

(1) Naval Research Laboratory, Code 7131, 4555 Overlook Drive SW, Washington DC 20375, (202) 767-7212, William.szymczak@nrl.navy.mil
(2) Code 6126, (202) 404-3389, Raymond.gamache@nrl.navy.mil

(U) Predictions of the amount of water thrown upward from shallow depth explosions are presented in support of a new water barrier concept for the protection of Riverine vessels. The predictions are obtained using a model based on a generalized formulation of hydrodynamics using an incompressible liquid assumption, which has been previously validated on a variety of applications including water plume predictions. Depending on both the charge weight and initial depth, this study presents estimates for the Effective Water Length (EWL) values at heights and time intervals relevant for riverine vessel protection from Rocket Propelled Grenade (RPG) attacks.

(U) INTRODUCTION

(U) A new water barrier concept is being investigated to support riverine vessel RPG survivability. A water barrier could protect maritime vessels against a large range of threats through the formation of an interposing wall of water. This is accomplished through the delivery and detonation of an explosive charge beneath the waterline (~2-3ft) along the incident threat trajectory 12 ft from a central point above the vessel, forming a literal water barrier that initiates and absorbs an incident shape charge jet. The water barrier system order of operation includes an IR detection of threat launch, radar trajectory tracking, intercept solution, engagement, water barrier formation, RPG initiation/jet formation, and jet. An additional benefit of this system is the minimal collateral damage caused by the water barrier where blast and fragmentation are mitigated underneath the waterline.

(U) The water barrier concept allows for the use of available maritime resources while relaxing the precision requirements for engagement timing and threat trajectory height determination. By using a simplified 2D threat trajectory, the use of low cost radar systems (less than $20,000) can be enabled. The relaxed engagement timing results from a large duration of time (~ 1.0 seconds) where the water barrier remains of adequate size to defeat incident RPGs. Initial shape charge jet performance studies against water show a requirement of 48” water depth to completely erode an initiated RPG-7 jet. Additional factors related to the dynamics during the water barrier formation may additionally reduce the required depth to erode the incident shape charge jet.

Approved for public release; distribution is unlimited

Report Documentation Page

Form Approved
OMB No. 0704-0188

1. REPORT DATE	2. REPORT TYPE	3. DATES COVERED
AUG 2014	**N/A**	**-**

4. TITLE AND SUBTITLE	5a. CONTRACT NUMBER
Water Barrier Predictions For Riverine Vessel Defense	5b. GRANT NUMBER
	5c. PROGRAM ELEMENT NUMBER
6. AUTHOR(S)	5d. PROJECT NUMBER
	5e. TASK NUMBER
	5f. WORK UNIT NUMBER
7. PERFORMING ORGANIZATION NAME(S) AND ADDRESS(ES) **Naval Research Laboratory, Code 7131, 4555 Overlook Drive SW, Washington DC 20375**	8. PERFORMING ORGANIZATION REPORT NUMBER
9. SPONSORING/MONITORING AGENCY NAME(S) AND ADDRESS(ES)	10. SPONSOR/MONITOR'S ACRONYM(S)
	11. SPONSOR/MONITOR'S REPORT NUMBER(S)

12. DISTRIBUTION/AVAILABILITY STATEMENT
Approved for public release, distribution unlimited

13. SUPPLEMENTARY NOTES
NDIA 2014 Warheads & Ballistics Symposium on 4-7 August 2014, held in Naval Postgraduate School, Monterey, CA

14. ABSTRACT

15. SUBJECT TERMS

16. SECURITY CLASSIFICATION OF:			17. LIMITATION OF ABSTRACT	18. NUMBER OF PAGES	19a. NAME OF RESPONSIBLE PERSON
a. REPORT	b. ABSTRACT	c. THIS PAGE			
unclassified	**unclassified**	**unclassified**	**SAR**	**12**	

(U) Water barrier formation combined with detection/engagement timing calculations show that the water barrier can defend against engagements as close as 149 ft (45 meters) (shooter to platform) at a water depth of 2-3 ft. The water barrier also removes fratricide/blast lethality, which is a key issue for lightly armored riverine vessels.

(U) It should be noted that the water barrier can be used in all brown and green water environments as the width of the engagement range (width beyond the vessel where water barrier is formed [12 ft]) of both sides of the riverine vessel is shorter than the length of the vessel (The riverine vessel typically requires a draft of 3 ft and river width wide enough to turn the vessel around).

(U) Within the water barrier effort there are currently multiple variables that must be studied and integrated to demonstrate the effectiveness in defeating an incident RPG threat. This paper will focus on the computational modeling of the water barrier formation through energetic initiation. Timing (formation/dwell) and Equivalent Water Length (EWL) will be studied as functions of: charge weight, detonation depth, wall height and physical boundary conditions. Additional studies of the ability to induce an upward angular velocity to the incident threat will also be performed.

(U) MODELING DETAILS

(U) The predictions shown in this study are obtained using a model based on a generalized formulation of hydrodynamics using an incompressible liquid assumption [1]. This formulation is well suited for predicting long-time bubble and plume dynamics for the several reasons. First of all, the "water" or "liquid" region is modeled as incompressible, thereby allowing for time steps proportional to the inverse of the water velocity as opposed to the much smaller time steps that a compressible formulation would require based on the speed of sound in water. This is important because plume behavior occurs on the order of seconds. Secondly, the model allows for regions of "spray," which is typical of plume behavior in which a well defined interface between the bubble and water or especially the water and the air does not exist. Finally, the computational model uses a fixed "Eulerian" grid providing for generality in studying complex bubble dynamics and free surface topology changes. For shallow-depth explosions this includes the underwater bubble forming one or more annular regions as a downward moving jet intersects the bottom surface of the bubble as it collapses, in addition to the radial plumes ejected on the bubble's second expansion, and the eventual venting of the bubble into the atmosphere.

(U) The generalized formulation of hydrodynamics is based on the solution of the mass and momentum conservation equations

$$\rho_t + \nabla \bullet (\rho \mathbf{u}) = 0 \tag{1}$$

$$(\rho \mathbf{u})_t + \nabla \bullet (\rho \mathbf{u}\mathbf{u}) = -\rho g \mathbf{k} - \nabla p \tag{2}$$

subject to the constraint

$$\rho \le \rho_0 , \tag{3}$$

where ρ is the time and spatially varying density, ρ_0 is the constant density of the incompressible liquid, $\mathbf{u}$ is the velocity vector, p is the pressure, and $\mathbf{k}$ is the unit vector in the direction of gravity, g. These equations are approximated using a split-step approach. First, the conservations equations (1) and (2) are approximated using an explicit second-order Godunov Method with monotonized slope limiting without regards to the constraint (3). The density constraint is then imposed through the solution of a variational inequality. We remark that the imposition of (3) also has an effect on the momentum, otherwise non-physical and numerically unstable energy increases may occur. The treatment of this constraint is one of the unique features of the generalized hydrodynamics formulation, distinguishing it from other approaches, which simply truncate the density, e.g. [2]. Finally, the pressure is determined using a projection method based on discretizations derived from a finite element method.

(U) These algorithms have been implemented within the computation codes BUB2D (for two dimensional and axially symmetric problems) and BUB3D for fully three-dimensional problems. Validations of these codes on a variety of applications including water plume predictions may be found in [1,3-5], as well as much more detail of the numerical procedures used.

(U) NUMERICAL RESULTS

(U) Computations were performed in an axially symmetric domain with $0 \le r \le R$, and $Z_B \le z \le Z_T$ where $z = 0$ corresponds to the ambient air-water free surface. The grids used for the computations were comprised of uniform square cells of size h in the sub-region $0 \le r \le 8$, $-10 \le z \le 10$ in units of feet. Outside of the uniform region the grids are stretched to the boundary of the domain in which $R = 40$, $Z_B = -20$ and $Z_T = 120$. In order to study the numerical errors, computations were performed using a "coarse" grid using a total of 120×400 cells with $h = 0.1$, and a "fine" grid using 240×800 cells with $h = 0.05$.

(U) Effective Water Length

(U) The results are presented using density contours at different times of the bubble evolution as well as measurements of the equivalent water length as a function of both height above the surface and time. For this analysis we consider the idealized case of a missile travelling along a horizontal line at a given height $z = z_H$. Setting the initial location of the charge at coordinates $(x_c, y_c, z_c) = (0,0,-d)$ and assuming that the missile travels on a straight line trajectory from $(-x_o, S, z_H)$ moving in the positive x-direction with an infinite velocity. Then the Equivalent Water Length for this trajectory at time *t* is

$$EWL(t, S, z_H) = \frac{1}{\rho_0} \int_{-x_0}^{\infty} \rho(t, x, S, z_H)\, dx \tag{4}$$

where ρ_0 is the ambient density of the water, $\rho(t, x, S, z_H)$ is the density of the spray (water-air) mixture at time, S is the offset of the trajectory from the charge center, and z_H is the height of the trajectory.

(U) The values for $\rho(t,x,S,z_H)$ will be approximated using an axially symmetric computation using the BUB2D code which produced values $\rho_{i,j}^n$ at discrete times $t = t^n$, at cell center locations (r_i, z_j) where $r = \sqrt{x^2 + y^2}$ is the distance from the axis. We can also express

$$EWL(t,S,z_H) = \frac{1}{\rho_0} \int_{-x_0}^{\infty} \rho_h(t, r(x,S), z_H)\, dx \tag{5}$$

The integral (5) is evaluated under the assumption that ρ_h is piecewise linear in time and piecewise constant in space using the computational values within each grid cell. Note that the maximum values of (5) will usually occur when $S = 0$ which will be evaluated as a "best case scenario". The goal of these predictions is to demonstrate conditions under which the *EWL* values are larger than 4 ft. at a height of 8 feet, for a sufficiently large time interval.

(U) Run Matrix

(U) The initial plan called for predictions using charge weights of 1, 1.5, and 2 lbs, at depths of 3, 4 and 5 feet. An important parameter for the behavior of shallow depth explosion is the scaled depth defined by

$$C = \frac{D}{A_{\max}} \tag{6}$$

The scaled depths corresponding to this set of tests are listed in Table 1. For some critical value of $C = C^* < 0.56$ the bubble gas will escape into the atmosphere during its first expansion and contraction phase. Although the critical value has not been precisely defined in the literature (e.g. Kedrinski [6] gives the value as 1, but Blake and Gibson [7] clearly show an example where $C = 0.56$ which does not vent). It is likely that the there is a transition region where the bubble partially vents into the atmosphere with the amount of venting depending C. In [8], Young gives the bound $C^* = 0.2$ below which the gas can be observed surrounding a central column of water in the plume. Experiments performed at the University of Maryland [9] using small-scale RP80 charges on a sandy bottom yielded an approximate value $C^* \approx 0.25$ in rough agreement with Young's estimate. Based on that data we expect little or no venting even for the range of trials listed in Table 1 where $C > 0.448$.

Table 1 — Scaled depths for the original run matrix.

	Charge Weight (lbs)		
Depth (ft)	1.0	1.5	2.0
3	0.565	0.493	0.448
4	0.760	0.664	0.603
5	0.959	0.838	0.761

We remark that these computations were extended to shallower depths, and these results will appear in a more extensive report, currently in preparation.

(U) Grid effects and Numerical error

(U) We begin by using the same resolution for the grids described in the previous section and approximate the known solution for the case of a spherical bubble in an infinite incompressible medium, governed by the Rayleigh-Plesset equation [10] with conditions set so that the ratio of the initial (minmum) and maximum bubble radius was $A_{\max} / A_{\min} = 13.28$ and the period of oscillation is $T_\infty = 0.372236$ s.

(U) For this infinite domain problem there are three sources of error, namely the nominal spatial discretization size *h*, the time step sizes and the boundary truncation. The time steps are selected adaptively based on changes in the bubble volume. The values listed in Table 2 compare the errors in the bubble period (time to first minimum) and bubble maximum radius from two separate computations of the infinite domain problem. In this table the value L is the distance from the computational boundary to the charge center, N_x is the number of cells used in each direction for the computation, N_T is the total number of time steps taken before the final time of $T_f = 0.4$. Note that the value of N_x on the fine grid is more than double the value on the coarser grid since the domain size was also doubled in each direction. The computational results are indicated by $A^h_{\max}$ for the maximum bubble radius and T^h for the first bubble period. The value $A^h_{\max}$ is determined from the maximum volume computed from the density field for a sphere of equivalent volume. The errors (*E*) are listed as relative errors between the computed values and the exact values listed above. These results indicate the accuracy of the code for obtaining the critical bubble dynamics parameters, which in turn affect the dynamics of shallow water plumes. For the computations of the shallow plume dynamics presented next, all the results were based on the $h = 0.05$ grid so that we expect approximately 1% error in the maximum equivalent bubble radius and about 4% for the period.

Table 2 — Symmetric bubble simulation results.

h	L	N_x	N_T	$A^h_{\max}$	$E\left(A^h_{\max}\right)$	T^h	$E\left(T^h\right)$
0.1	50	140	823	6.5735	1.77%	0.3448	7.38%
0.05	100	400	1581	6.6382	0.81%	0.3567	3.94%

(U) Fig. 2 displays the difference from the coarse and fine grids for the case for a 2 lb. charge weight and an initial depth of 3 feet (W2D3) at early times $t \le 0.5$ s . This represents a shallow depth non-venting case. The top row displaying the contours resulting from the coarse grid, and the corresponding fine grid results immediately below. The results from both grids are qualitatively very similar, with each predicting a central plume above the bubble at $t = 0.1$ s when the bubble is near its maximum volume. As the bubble begins to compress a downward moving plume is seen piercing through the bubble and impacting the bottom surface at $t = 0.2$ s. During the next re-expansion radial plumes are ejected surrounding the central plume as seen at $t = 0.5$ s. The evolution of the plumes rising and falling at later times $t \ge 1$ s are matched very well on each grid as seen comparing the top (coarse grid) and bottom (fine grid) rows. The relative density palette used for the contours are shown below the frame images in both figures, so that blue corresponds to pure water, and white corresponds to void, and regions of "spray" between the two.

U) Water Barrier Measurements

(U) For the water barrier measurements we computed the values $EWL(t,0,z)$ given by (5) through the center of the plume using a density contour plot shown in Fig. 3 for the D3W2 case using the fine grid. Below the *EWL* contour are the corresponding density contours at various dis-

crete times and heights from 0 to 10 feet above the surface. In the contour plot, *EWL* values larger than 5 are simply shown as light red as indicated in the palette on the right.

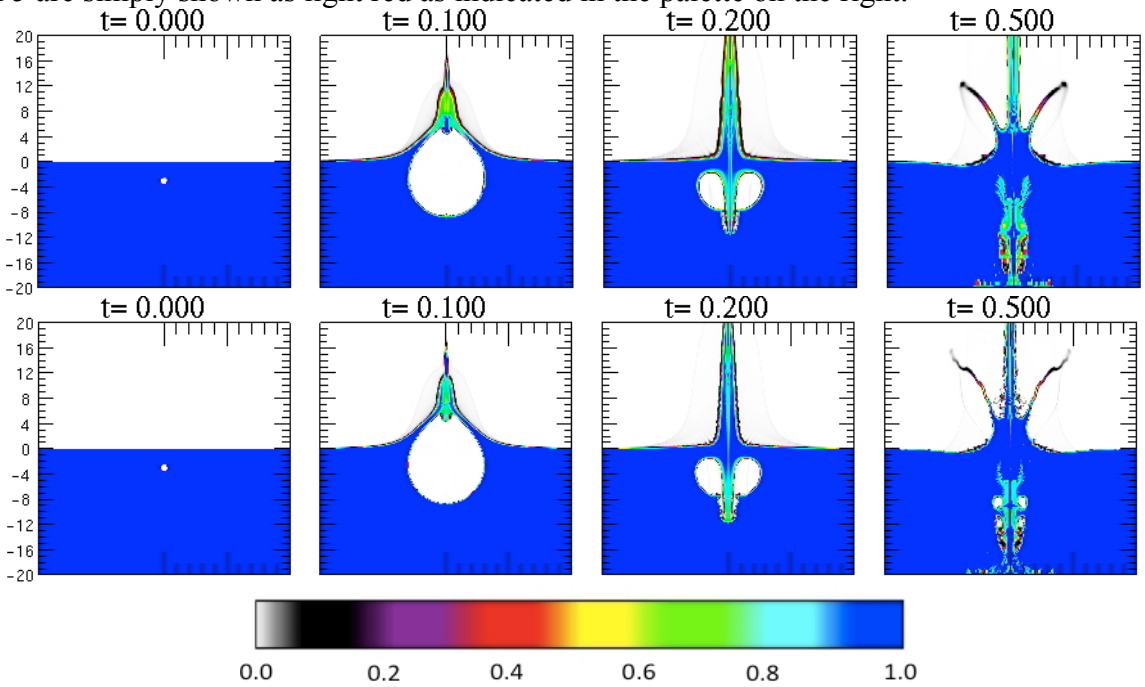

Fig. 2.(U) Run W2D3 coarse (top) and fine (bottom) grid density contours at early times.

(U) The contours of *EWL* values for the original run matrix in Table 1 are shown in Fig. 4. This figure clearly indicates higher *EWL* values for larger charges and shallower depths within this range. Furthermore, according to the scaled depths listed in Table 1, we would expect similar behavior from the case W1D4 and W2D5 (with both length and time scaled by the factor $\sqrt[3]{2} \approx 1.26$). This is clearly reflected in Fig. 4, as well as the similarity between the W1D3 and W2D4 case. This scaling is not exact since gravity will have a slightly greater influence in the larger charge case. Plots of the computed values $EWL(t,0,H)$ for $H = 4$, 6, and 8 for the run matrix are shown in Figure 5. None of these cases produced values that attained the desired value of 4 ft at the $H = 8$ ft height level, but this value is attained at $H = 4$ ft, for charge weights $W \geq 1.5$.

(U) Plume Velocity

(U) The plume velocity may also enhance its protective ability as a barrier, potentially deflecting a missile by imparting a vertical momentum. The vertical velocity component along the axis, $v(t,0,H)$, is shown in Fig. 6 for the same cases as shown for the *EWL* values in Fig. 5. Note the large negative downward velocities reported at the lower $H = 4$ ft height at early times. These negative velocities indicate the downward jet seen during the beginning of the first bubble contraction shown in Fig. 2 at times $t = 0.1$ and $t = 0.2$ seconds. The upward moving jet can be expected to attain speeds of 100 ft/s or larger, during the time of the first bubble expansion, after which it is decelerated primarily due to gravity. We remark that here we are only showing the vertical velocities along the axis, and are thereby ignoring the velocity of the radial plumed ejected during the beginning of the second bubble expansion.

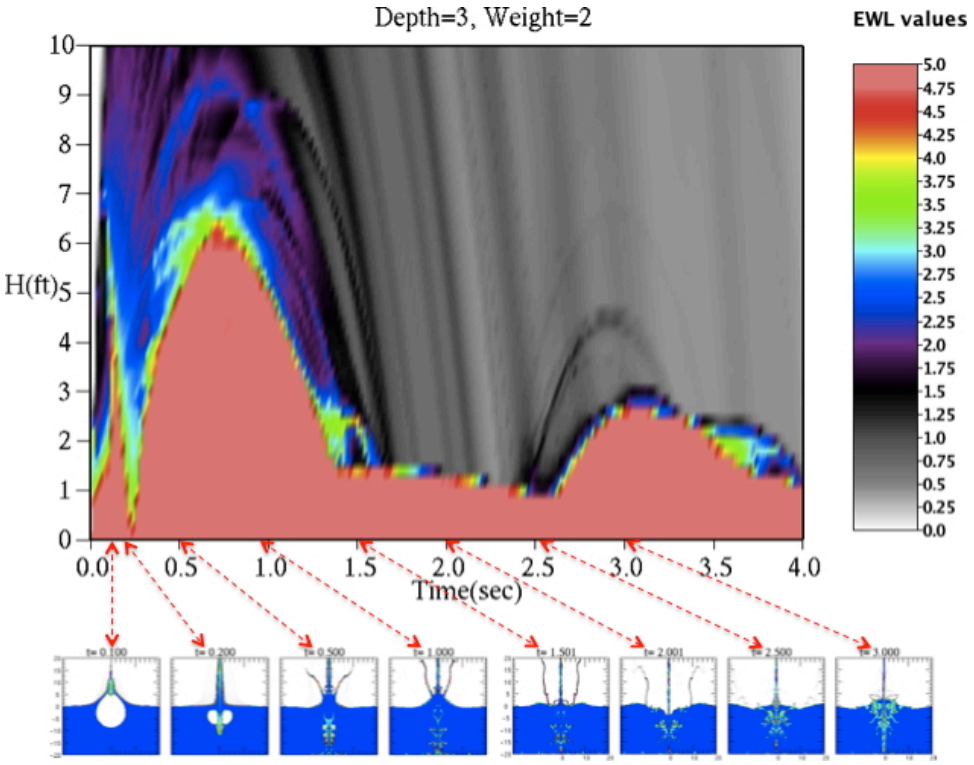

Fig. 3.(U) EWL Contours with Plume events for the W2D3 case.

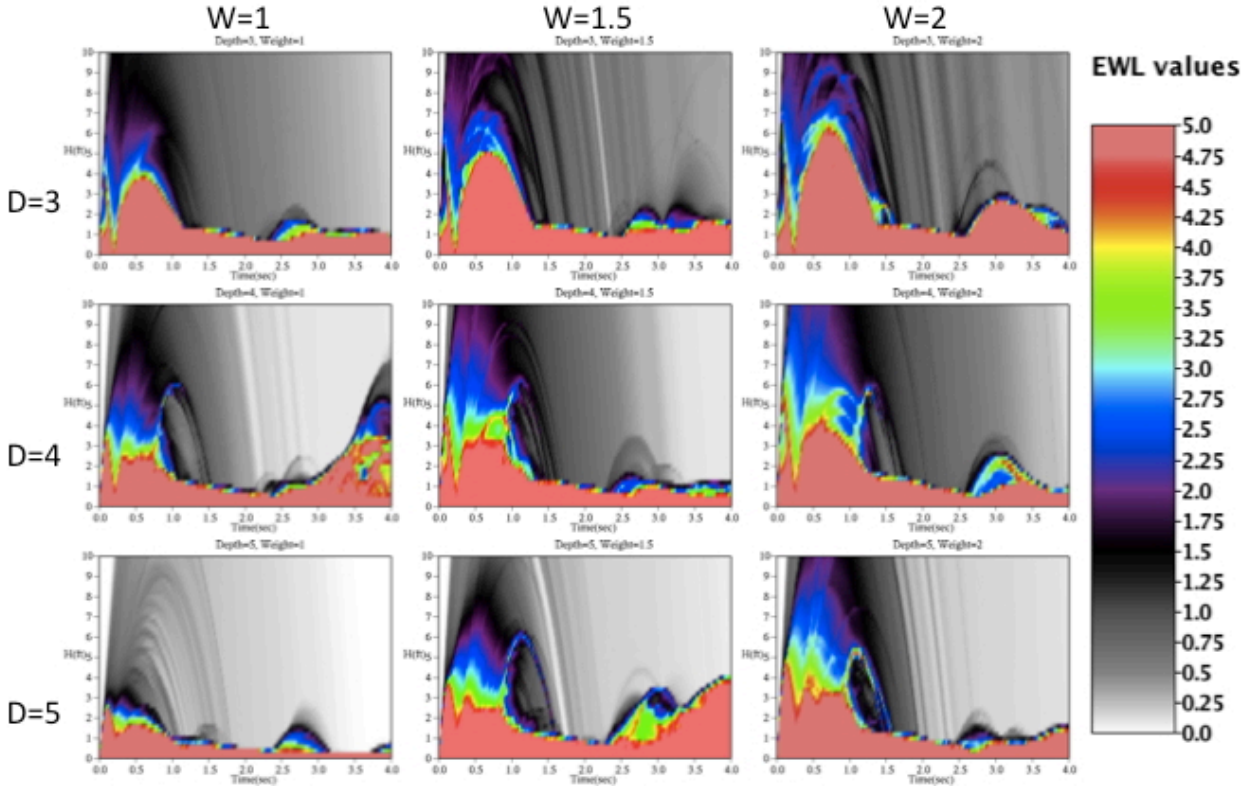

Fig. 4. (U) Comparison of EWL contour levels for the original run matrix.

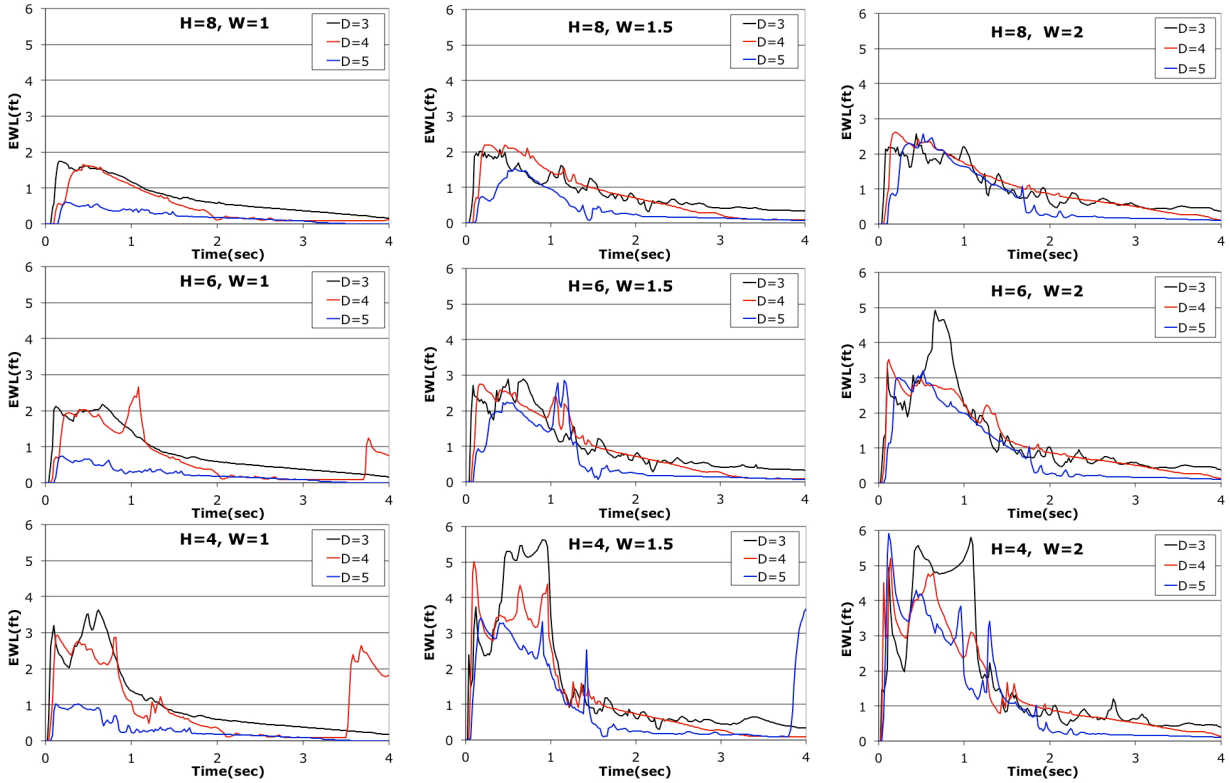

Fig. 5. (U) EWL values as a function of time at different heights for the original run matrix

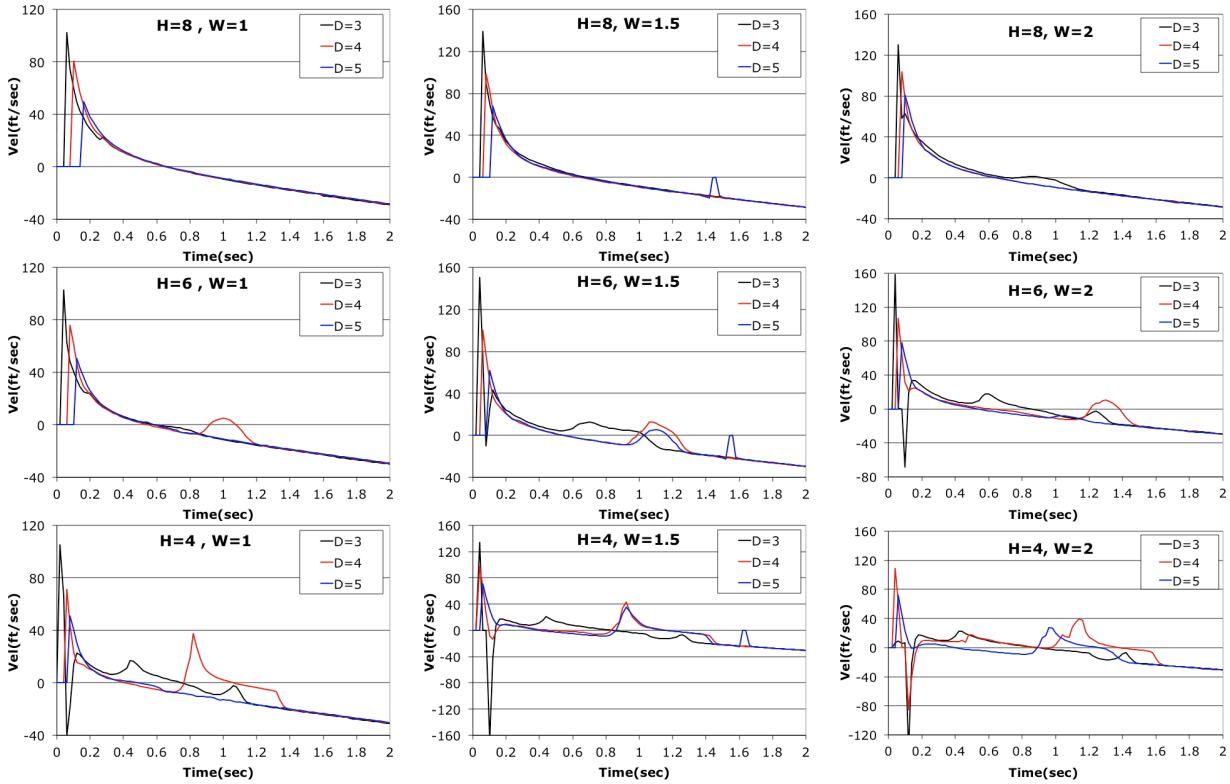

Fig. 6.(U) Vertical plume velocities at different heights for the original run matrix

(U) Boundary Effects

(U) The effects of two different boundary regions were also compared to the $z \geq Z_B = -20$, cases described above. For these comparisons the charge weight was fixed at $W = 2$ lbs, and the initial depth was set at $D = 3$ ft. In the first case, the initial water region was restricted to a cylindrical "pool" having dimensions $r \leq R = 9$ and $0 \geq z \geq Z_B = -8$. The purpose of this simulation was for a preliminary investigation for designing test experiments in a controlled environment. In the second case only the bottom boundary was changed so that $0 \geq z \geq Z_B = -3$. In this case the initial bubble was the top half of a hemisphere situated at the bottom boundary. The hemisphere has the same volume as the initial bubble for a spherical charge region. In each case the grid was chosen to match the original fine grid with uniform cells of size $h = 0.05$ for $z \leq 10$ and $r \leq 8$.

(U) Fig. 7, exhibits the early time plume and bubble contours for the original domain compared to the two restricted domain cases. A comparison of the corresponding EWL contours shown in Fig. 8, indicate that both restricted domains increase the amount of water thrown upward. In the original domain the water surrounding the charge is pushed outward nearly spherically in each direction. In the case of shallow water when the charge is sitting at the bottom boundary, all of the water is pushed upward or radially outward (hemispherically). Thus, more water can be expected to be pushed upward than in the original domain (since the total volume displaced will be about the same, but none will be displaced downward). In the case of the confined pool, a significant portion of the radial velocity is converted to vertical velocity at the pool side boundaries, again causing more water to be directed upward. Based on these observations, we conjecture that the case of a shallow plume in free water represents the case of lowest *EWL* values.

(U) SUMMARY AND CONCLUSIONS

(U) This report presents a numerical investigation of the amount of water ejected from shallow depth explosion plumes for the potential use as a barrier from incoming projectiles. The computational code BUB2D was used for the simulations based on the generalized hydrodynamics model which has been verified and validated on a wide variety of applications, including shallow plume simulations (see, e.g. [1,3-5]). The parameters used for the code in this report were selected such that the transition from a non-venting to venting bubble occurred at the approximate scaled depth value $C = D / A_{\max} \approx 0.25$, consistent with values reported in [8]. Using these same parameters and the same initial conditions as the shallow plume simulations, a grid convergence study was performed on the spherically symmetric bubble, demonstrating the errors were under 1% for the bubble maximum radius, and less than 4% for the first period.

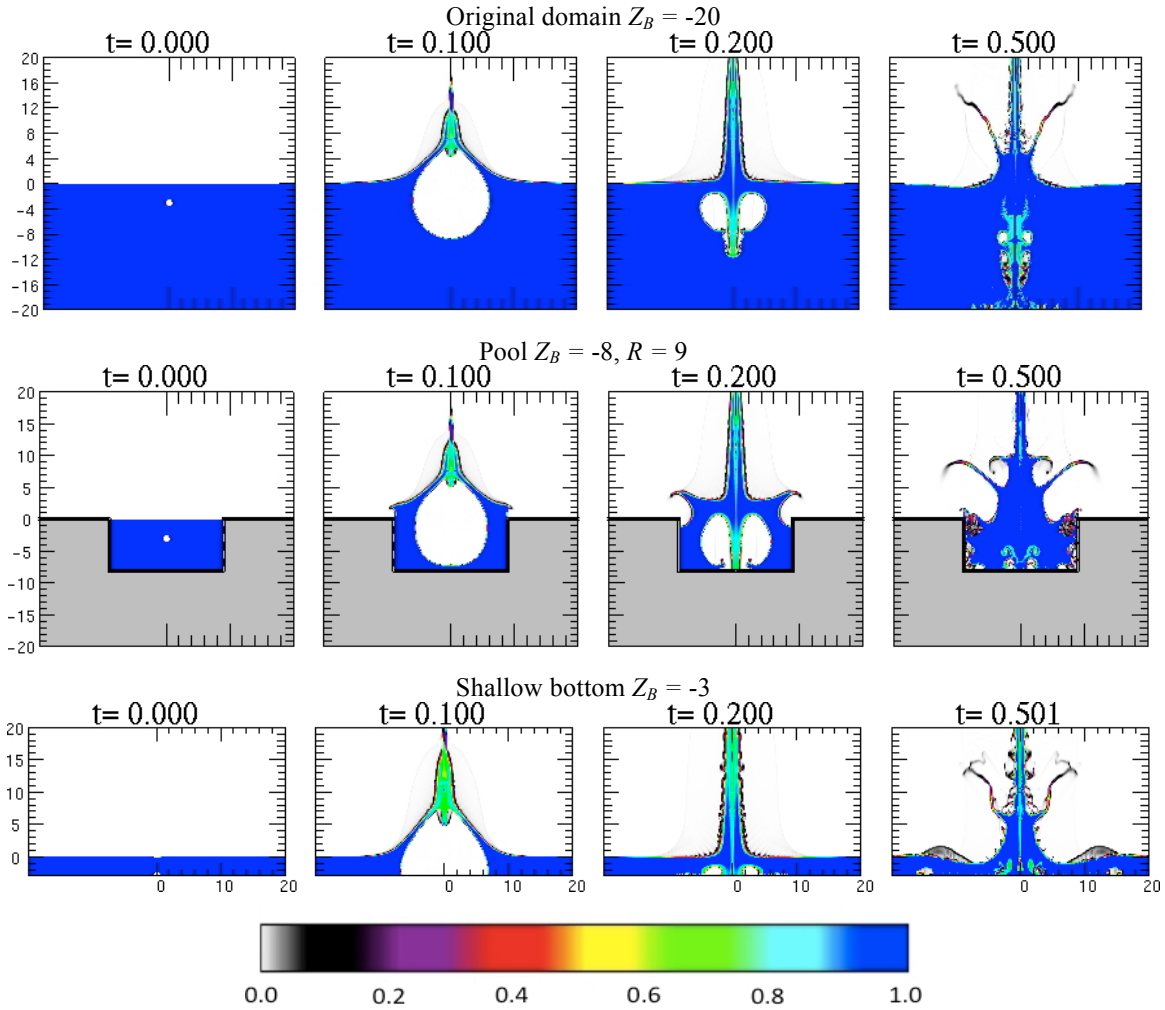

Fig. 13. (U) Early time boundary effects W2D3 case.

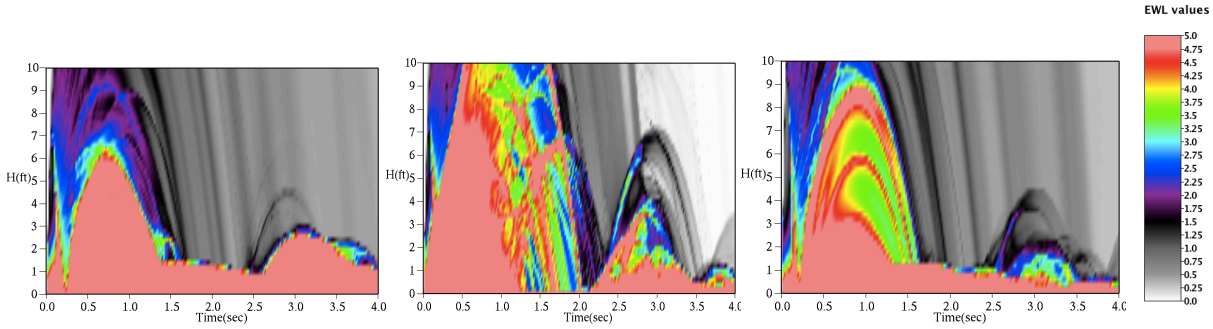

Original domain Pool confinement Shallow bottom

Fig. 14. (U) *EWL* contours for the W2D3 case with different boundaries.

(U) The simulations for the original run matrix (charge weights between 1 and 2 pounds, and charge depts. Between 3 and 5 feet) revealed just over a peak equivalent length of between 1 and 3 feet of water through the plume center is ejected when measured at a height of 8 feet above the surface. These barriers increased to between 2 and 5 feet when measured at a height of 6 feet, and between 3 and 6 feet at a height of 4 feet above the surface. The peak plume velocities were on the order of 100 ft/s, but these decayed after the time of the first bubble maximum volume at approximately $t = 0.1$ seconds.

(U) The effects of shallow depths, and constrained regions were shown to slightly enhance the *EWL* levels. In the first case this demonstrates that if an effective barrier is formed in deep water, it will remain effective in shallow water, provided the depth is not so shallow that the bubble vents. The case of the restricted "pool" shows some consideration must be given if any validations are performed in a confined experimental region.

(U) Future Studies

(U) The results presented here represent a starting point for the feasibility of designing an effective protection system for riverine vessels. There are several critical issues and studies that have not yet been addressed or performed. These include

1. Further model validations. The best validations are from comparisons to actual experiments. However, determining *EWL* values accurately is not trivial as demonstrated in the early attempts discussed in [11-13]. In particular, consistency of the data using different measurement techniques was not adequately demonstrated. Alternatively, the current model can be compared to other models which have also been validated for underwater explosion problems. One such code is DYSMAS [14] which is a more general hydrocode than BUB2D, and includes a compressible equation of state for water, thereby treating shock effects directly.
2. Off center plumes. The EWL values reported here represented the best case since they were determined by integrating in a straight line through the plume center ($S = 0$). The sensitivity of the measurements on the case when the plume is not in the direct path of the plume center $S > 0$ is not addressed here.
3. Plume velocity effects. The velocity measurements were done for the purpose of future including the momentum imparted on the incoming missiles due to the vertical velocity of the plumes. Some of these velocities were included in Fig. 6, but the analysis of its effect on vehicle protection have not been addressed.
4. Water entry effects. The water barrier concept in consideration involves the entry of a charge fired into the water between the vessel and incoming missile. The water entry event is expected to form a trailing cavity behind the projectile which will probably not close before the charge detonates. The effects of this cavity on the subsequent bubble and plume formation has not been investigated.

(U) Addressing these topics will enable the reliable assessment of the water barrier protection system. With accurate simulation tools, system performance can be optimized, without the need of conducting a large number of field trials.

(U) REFERENCES

1. W.G. Szymczak, J.C.W. Rogers, J.M. Solomon, and A.E. Berger, "A Numerical Algorithm for Hydrodynamic Free Boundary Problems," *J. Comp. Phys.* **106**, 319-336, 1993.

2. C. W. Hirt, and B. D. Nichols, "Volume of Fluid (VOF) Method for the Dynamics of Free Boundaries," *J. Comp. Phys*. **39**, 201-225, 1981

3. W.G. Szymczak and J.M. Solomon, "Computations and Experiments of Shallow Depth Explosion Plumes," NSWCDD/TR-94/156, Naval Surface Warfare Center, Dahlgren Division, Dahlgren, Va., 1996.

4. J.C.W. Rogers and W.G. Szymczak, "Computations of Violent Surface Motions: Comparisons with Theory and Experiment," *Phil. Trans. R. Soc. Lond.* **355**(A), 649-663, 1997.

5. W.G. Szymczak, S. L. Means, and J.C.W. Rogers, "Computations pf bubble formation and pulsations generated by impacting cylindrical water jets," *Journal of Engineering Mathematics* **48**: 375-389, 2004.

6. V.K. Kedrinskii, "Surface Effects from an Underwater Explosion (Review)," *J. of Appl. Mech. and Tech. Phys.* **19**(4), 474-491 (1979).

7. R. Blake, B.B. Taib, and G. Doherty, "Transient Cavities near Boundaries. Part 1. Rigid Boundary," *J. Fluid Mech.* **170**, 479-497 (1986).

8. G.A. Young, "Dispersion of the Chemical Products of Underwater Explosions," NSWC TR 82-404, Naval Surface Weapons Center, Dahlgren, Va., December, 1984.

9. W.L. Fourney, D.J. Goodings, R.J. Bonenberger,, and H.U. Leiste, "Visualization of Cratering in an Underwater Environment," FRAGBLAST: The International Journal of Blasting and Fragmentation, 6, (1), 1-20, (2002).

10. R.H. Cole, *Underwater Explosions* (Princeton University Press, Princeton, N.J., 1948) Ch. 8, pp. 270-353.

11. J.T. Choe, K.A. Boulais, K.A. Chun, and K.A. Irwin, "Microwave Probe for Mass Measurements of a Water Plume," NSWCDD/TR-95/187, Naval Surface Warfare Center, Dahlgren Division, Dahlgren, Va., 1995.

12. L. Lipton, "Probe Measurement of Water Mass of Plumes Produced by Underwater Detonations," IHTR 1757, Naval Surface Warfare Center, Indian Head Division, Indian Head, Md., 1995.

13. W.G. Szymczak and C.E. Higdon, "Model Validations and Predictions for Water Barrier Defense," NRL/FR/7130—98-9880, Naval Research Laboratory, Washington, DC, 1998.

14. DYSMAS User's Manual, NSWC Indian Head Division, Indian Head, MD, DYSMAS Verison 6.5.03, 30 April, 2013.